Role of the Plasmoid Instability in Magnetohydrodynamic Turbulence

Chuanfei Dong,[1,2,*] Liang Wang,[1,2] Yi-Min Huang,[1,2] Luca Comisso,[1,2,3,4] and Amitava Bhattacharjee[1,2]

[1]*Department of Astrophysical Sciences, Princeton University, Princeton, New Jersey 08544, USA*
[2]*Princeton Plasma Physics Laboratory, Princeton University, Princeton, New Jersey 08540, USA*
[3]*Department of Astronomy, Columbia University, New York, New York 10027, USA*
[4]*Columbia Astrophysics Laboratory, Columbia University, New York, New York 10027, USA*

The plasmoid instability in evolving current sheets has been widely studied due to its effects on the disruption of current sheets, the formation of plasmoids, and the resultant fast magnetic reconnection. In this Letter, we study the role of the plasmoid instability in two-dimensional magnetohydrodynamic (MHD) turbulence by means of high-resolution direct numerical simulations. At a sufficiently large magnetic Reynolds number ($R_m = 10^6$), the combined effects of dynamic alignment and turbulent intermittency lead to a copious formation of plasmoids in a multitude of intense current sheets. The disruption of current sheet structures facilitates the energy cascade towards small scales, leading to the breaking and steepening of the energy spectrum. In the plasmoid-mediated regime, the energy spectrum displays a scaling that is close to the spectral index -2.2 as proposed by recent analytic theories. We also demonstrate that the scale-dependent dynamic alignment exists in 2D MHD turbulence and the corresponding slope of the alignment angle is close to 0.25.

Introduction.—Magnetohydrodynamic (MHD) turbulence plays a fundamental role in the transfer of energy in a wide range of space and astrophysical systems, from the solar corona [1,2] and accretion disks [3,4], to the interstellar medium [5,6] and galaxy clusters [7,8]. Indeed, in all these environments, MHD turbulence is responsible for the transfer of energy from the large scales where energy is provided to the small scales where it is dissipated. Establishing a detailed understanding of MHD turbulence is a pivotal but yet unresolved problem, with far-reaching repercussions in many research areas.

An important feature of MHD turbulence is the tendency to develop sheets of strong electric current density [9–19]. These current sheets are natural sites of magnetic reconnection, leading to the formation of plasmoids that eventually disrupt the sheetlike structures in which they are born [20–29]. The first analytic calculation of the impact of plasmoid formation on the MHD turbulent cascade is attributable to Carbone, Veltri, and Mangeney [30], who proposed that current sheet structures in a turbulent environment disrupt when $\gamma \tau_{\mathrm{nl}} \sim 1$, with τ_{nl} and γ corresponding to the nonlinear eddy turnover time and the growth rate of the fastest tearing mode, respectively. Under this condition, they derived a length scale at which the inertial range of turbulence breaks and found that the energy spectrum steepens because of the plasmoid instability. Interestingly, by performing hybrid-kinetic simulations, Refs. [27,28] showed that plasmoids can also directly contribute to the formation of a fully developed turbulent spectrum across the so-called ion break. To date, there have

been several attempts to further predict the disruption criteria and the energy spectrum in the plasmoid-mediated regime [31–39].

Despite a series of analytic studies predicting a break of the energy spectrum caused by the plasmoid instability, no definitive evidence has been provided by direct numerical simulations of MHD turbulence so far. This is mainly due to the limitation of computational resources enabling the high magnetic Reynolds numbers that are required to achieve a regime where the plasmoid formation is statistically significant to affect the turbulent energy cascade. This Letter aims to address this problem by performing numerical simulations at unprecedented large magnetic Reynolds numbers (up to $R_m = 10^6$). Although recent theoretical arguments are based on three-dimensional turbulence, we will consider a two-dimensional scenario. In this way, we can achieve high resolution to resolve the plasmoid instability associated with the high R_m and observe a concomitant alteration in the spectrum of the turbulent cascade. According to our simulations, we demonstrate that plasmoids can cause a steepening of the energy spectrum, which exhibits a slope that is close to a value of -2.2.

Method.—The governing equations of our numerical model are the dimensionless viscoresistive MHD equations:

$$\partial_t \rho + \nabla \cdot (\rho \mathbf{u}) = 0, \tag{1}$$

$$\partial_t(\rho \mathbf{u}) + \nabla \cdot (\rho \mathbf{u}\mathbf{u}) = -\nabla(p + B^2/2) + \nabla \cdot (\mathbf{B}\mathbf{B}) + \nu \nabla^2(\rho \mathbf{u}), \tag{2}$$

$$\partial_t p + \nabla \cdot (p\mathbf{u}) = (\gamma - 1)(-p\nabla \cdot \mathbf{u} + \eta \mathbf{J}^2), \quad (3)$$

$$\partial_t \mathbf{B} = \nabla \times (\mathbf{u} \times \mathbf{B} - \eta \mathbf{J}), \quad (4)$$

where ρ, $\mathbf{u}$, and p are the mass density, velocity, and pressure of the plasma, respectively; $\mathbf{B}$ is the magnetic field and $\mathbf{J} = \nabla \times \mathbf{B}$ denotes the electric current density. The kinematic viscosity and the magnetic diffusivity are denoted as ν and η, respectively, while γ is the adiabatic index.

We solve Eqs. (1)–(4) using the BATS-R-US MHD code [40] in a domain $\{(x, y) : -L_0/2 \leq x, y \leq L_0/2\}$, where L_0 is set to unity. Periodic boundary conditions are employed in both directions. Lengths are normalized to the box size L_0, velocities to the characteristic Alfvén speed V_A, and time to L_0/V_A. We initialize the simulations by placing uncorrelated, equipartitioned velocity and magnetic field fluctuations in Fourier harmonics. More specifically, we set the initial velocity $u_x = \sum a_{mn} n \sin(k_m x + \xi_{mn}) \cos(k_n y + \zeta_{mn})$ and $u_y = \sum -a_{mn} m \cos(k_m x + \xi_{mn}) \sin(k_n y + \zeta_{mn})$, where m and n indicate the mode numbers in x and y directions; the wave number $k_m = 2\pi m/L_0$, and ξ_{mn} and ζ_{mn} are random phases. Energy is initialized in the range $l_{\min} \leq (m^2 + n^2)^{1/2} \leq l_{\max}$, where $l_{\min} = 1$ and $l_{\max} = 10$ with $a_{mn} = u_0/[(m^2 + n^2)(l_{\max}^2 - l_{\min}^2)]^{1/2}$. We set the magnetic field in the same way, with the constant u_0 replaced by B_0 and with different random phases. The out-of-plane magnetic field is set to zero; hence, there is no mean magnetic field. The constants u_0 and B_0 determine the strength of the initial velocity and magnetic fields. We set $u_0 = B_0 = 2$, which gives the initial energy $E = \frac{1}{2}\langle |\mathbf{u}|^2 + |\mathbf{B}|^2 \rangle \simeq \frac{1}{8}(u_0^2 + B_0^2) = 1$, where $\langle \cdots \rangle$ represents the spatial average. The plasma density and pressure are initially set to constant values $\rho = 1$ and $p = 10$, respectively.

We performed simulations with different values $(4 \times 10^4, 8 \times 10^4, 1 \times 10^5, 2 \times 10^5, 1 \times 10^6)$ of the magnetic Reynolds number, given by $R_m = u_0 L_0/\eta$. We vary the number of grid points from 2000^2 to 64000^2 for convergence study, ensuring the resolution is high enough to resolve the plasmoid instability associated with the highest R_m. Our analyses are based upon two cases: $R_m = 8 \times 10^4$ and $R_m = 1 \times 10^6$, with 64000^2 grid points. For the two cases, the magnetic diffusivity and viscosity are chosen to be (1) $\eta = 2 \times 10^{-6}$, $\nu = 1 \times 10^{-6}$ and (2) $\eta = 2.5 \times 10^{-5}$, $\nu = 1.25 \times 10^{-5}$; therefore, the magnetic Prandtl number $P_m = \nu/\eta = 0.5$. We analyze our data from the snapshot near the peak of the mean-square current density $\langle J_z^2 \rangle$, when the turbulence is fully developed $(t \sim 0.2)$.

Results.—Figure 1 depicts the simulated J_z with $R_m = 1 \times 10^6$, and displays coherent structures with intermittent intensity. In order to show plasmoids formed within the time-evolving current sheets (e.g., Refs. [32,34,35]), we zoom into the selected regions. It is noteworthy that the plasmoids grow locally within the current sheets in our
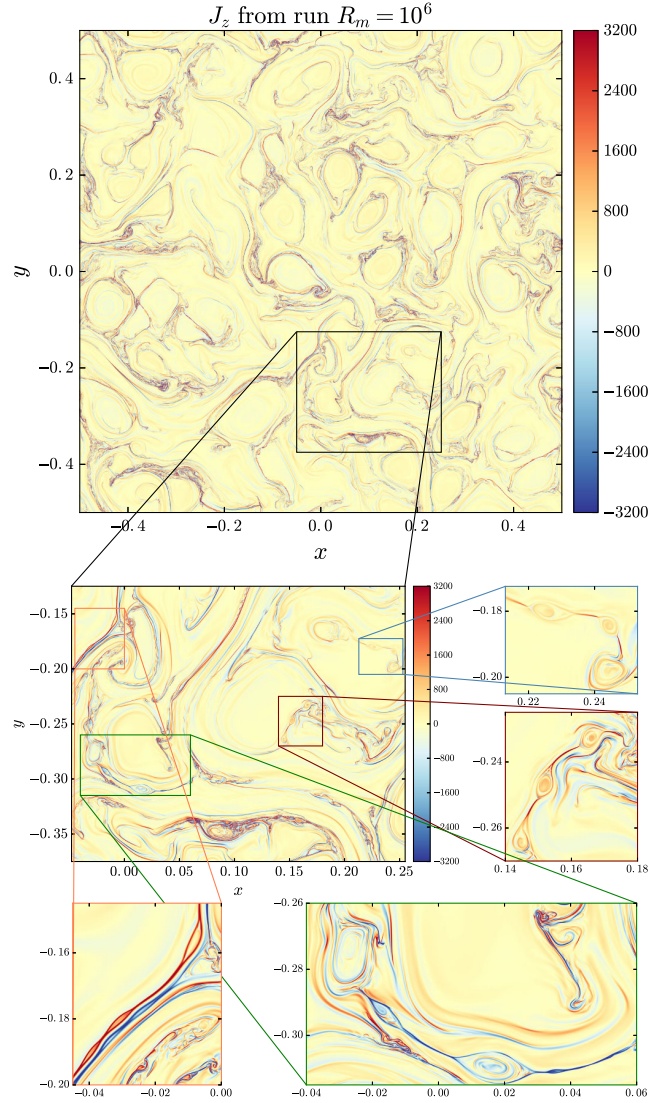

FIG. 1.   2D contour plots of the current density J_z at $t = 0.2$ for the simulation with magnetic Reynolds number $R_m = 1 \times 10^6$. Zoomed-in subdomains are used for the illustration of plasmoids. Copious formation of plasmoids occurs in multiple intense current sheets because of the plasmoid instability.

simulation [41], instead of being convected into the current sheets by finite amplitude fluctuations [20,25]. Chains of plasmoids are formed at different evolution stages in multiple intense current sheets. As will be discussed below, the disruption of the current sheet structures due to plasmoids can alter the turbulence energy spectrum by facilitating the energy cascade toward small scales. In contrast, Fig. 2, where $R_m = 8 \times 10^4$, reveals that plasmoids barely form in the same zoomed-in regions. The current sheet intensity for the low R_m case is significantly lower than that of the high R_m case. This is because the low R_m (equivalent to the Lundquist number, $S = V_A L_0/\eta$, in this study) prevents the current sheet from further thinning to smaller scales.
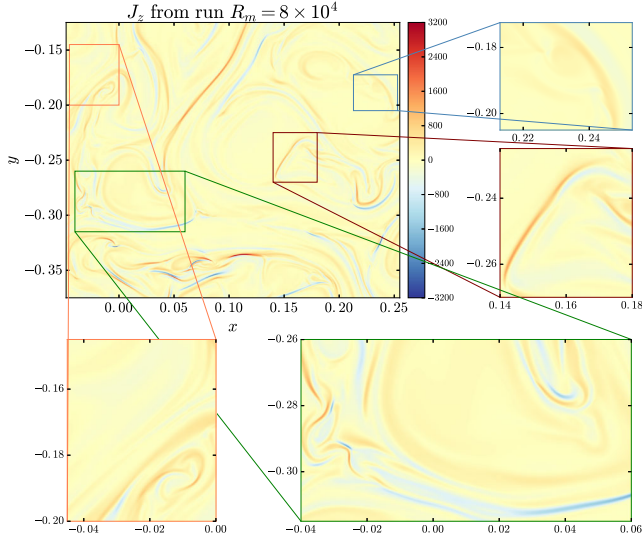
FIG. 2. 2D contour plots of the current density J_z (by choosing the same zoomed-in boxes and identical color bar range as that of Fig. 2) at $t = 0.2$ for the simulation with magnetic Reynolds number $R_m = 8 \times 10^4$. Barely any plasmoids can be observed in the current sheets due to the relatively low R_m that prevents the current sheet from further thinning; therefore, less intense current sheets develop in this simulation.

We now examine the turbulence energy cascade by computing the magnetic energy spectra, as shown in Fig. 3. The start of the inertial range, the transition scale between the standard inertial range and the plasmoid-mediated range, and the dissipation scale are denoted as k_i, k_*, and k_d, respectively. The low and high R_m simulations share the same k_i as a result of the identical initial setup except the distinct η and ν. In the low R_m case, k_* is absent or indistinguishable from k_d due to the small scale separation. Compared with the high R_m simulation, the spectrum of the low R_m case has a shorter inertial range and falls more quickly into the dissipation range. For the longer inertial range of the high R_m case, the formation of the plasmoids breaks the energy spectrum. The standard inertial range is characterized by a spectral index of -1.5, in accordance with Refs. [42,43]. For $k > k_*$ the spectrum becomes steeper and close to a spectral index of -2.2 [44], as recently proposed in Refs. [38,39] (also see Ref. [36], where the spectrum was proposed to be bounded between the spectral indexes $-5/3$ and -2.3). This sub-inertial range is only displayed in the high R_m case due to the copious formation of plasmoids that characterizes this simulation. The co-occurrence of both plasmoids and a steeper spectral index in the high R_m case is a reasonable indication that the steepening of the energy spectrum results from the disruption of the current sheet structures caused by plasmoids, which facilitates the energy cascade toward small scales.

Previously, the tendency of forming elongated, plasmoid-prone current sheets at small scales had been
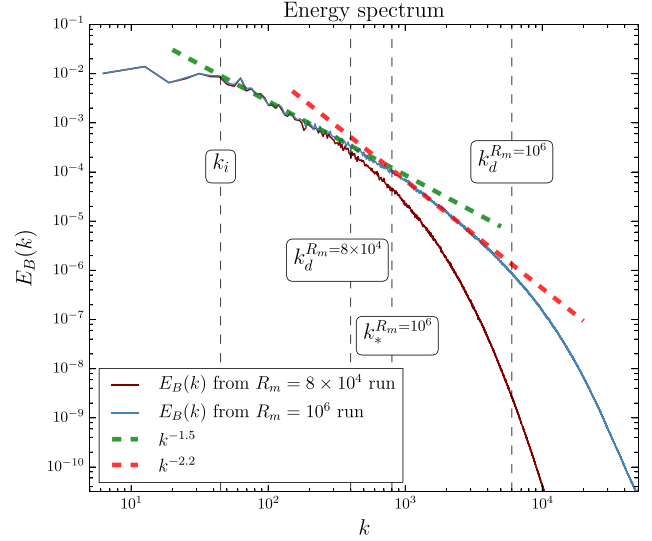
FIG. 3. Magnetic energy spectrum of the MHD turbulent cascade. k_i is approximately the start of the inertial range, k_d represents the dissipation range, and k_* indicates where the spectrum breaks and thus the start of the subinertial range. Both R_m cases share the same k_i. In the low R_m case, k_* is absent or indistinguishable from k_d due to the short scale separation. We choose k_i based on the left edge of the fitted power-law spectrum. k_* is determined by the intersection of the two fitted power-law spectra [45]. We estimate k_d by the condition that $\eta \int_0^{k_d} E_B(k)k^2 dk$ accounts for approximately half of the resistive dissipation power $\eta \langle J^2 \rangle$.

attributed to the effect of dynamic alignment [46], with an underlying assumption that the alignment angle can be employed as a proxy for current sheet inverse aspect ratio [36,37,39]. We measure the dynamic alignment angle θ_r as a function of the spatial separation between two sampling points, Δr, according to the definition $\sin \theta_r = \langle |\delta \mathbf{u} \times \delta \mathbf{B}| \rangle / \langle |\delta \mathbf{u}||\delta \mathbf{B}| \rangle$ given by Ref. [47]. Here, $\delta \mathbf{B} = \mathbf{B}(\mathbf{r} + \Delta \mathbf{r}) - \mathbf{B}(\mathbf{r})$ is the difference in the magnetic field between two points randomly sampled throughout the entire domain; likewise, $\delta \mathbf{u}$ is the difference in the velocity. The results, shown in Fig. 4, indicate that the alignment angle is close to $\theta_r \propto \Delta r^{0.25}$ for a wide range of Δr. This scaling relation is analogous to the one that characterizes 3D MHD turbulence [46], implying that the dynamic alignment may be universal in MHD turbulence regardless of the spatial dimensions. At a small spatial separation Δr, the higher R_m simulation is distinguished by a smaller θ_r than the low R_m one. This indicates that the high R_m case is associated with a higher current sheet aspect ratio based on statistics as expected.

Although the alignment angle progressively diminishes as the spatial separation decreases, the rather moderate alignment with $\theta_r > 0.1$ yields an aspect ratio no more than $O(10)$, which appears too low to cause the onset of the plasmoid instability. On the other hand, the existence of elongated and intense current sheets (see Fig. 1), despite the
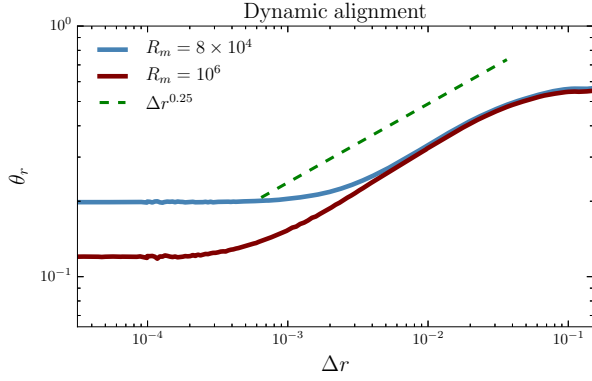
FIG. 4. The alignment angle θ_r in a log-log scale as a function of the spatial separation Δr. The dashed line indicates the scaling law $\theta_r \propto \Delta r^{0.25}$. The higher R_m case has a smaller alignment angle θ_r, especially at small spatial separations.

moderate values of the dynamic alignment, indicates that intermittency may play a key role [11]. In particular, MHD turbulence is known to be more intermittent in 2D than in 3D [12]. Given that Fig. 4 only presents an averaged picture of the dynamic alignment, we further define an alignment angle $\tilde{\theta}_r$ for an individual pair of $\delta\mathbf{u}$ and $\delta\mathbf{B}$ with $\sin\tilde{\theta}_r = |\delta\mathbf{u} \times \delta\mathbf{B}|/(|\delta\mathbf{u}||\delta\mathbf{B}|)$. Figure 5(a) depicts the probability density functions (PDFs) of $\tilde{\theta}_r$ calculated at separations determined by k_i, k_*, and k_d as indicated in Fig. 3. At the scale of k_i, the PDFs of both R_m cases have a relatively uniform distribution spanning over all the alignment angles, indicating the alignment angle at the k_i scale is nearly isotropic. As the separation Δr decreases, the nonuniformity in the PDF gets amplified and the mean value of the alignment angle shifts to smaller $\tilde{\theta}_r$. At the k_d scale, the higher R_m case exhibits more anisotropy than the lower R_m case. Notably, there exists a substantial probability for the individual alignment angle $\tilde{\theta}_r$ to be significantly smaller than the averaged alignment angle θ_r shown in Fig. 4.

To further quantify intermittency, we analyze the PDFs of magnetic field increments $|\Delta_{\Delta r}\mathbf{B}| = |\mathbf{B}(\mathbf{r} + \Delta\mathbf{r}) - \mathbf{B}(\mathbf{r})|$ for various Δr [48]. In Fig. 5(b), we show the PDFs of the x component $\Delta_{\Delta r}\mathbf{B_x}$ at the same separations as Fig. 5(a). PDFs of $\Delta_{\Delta r}\mathbf{B_y}$, not shown here, are analogous to that of $\Delta_{\Delta r}\mathbf{B_x}$. The PDFs at the dissipation scale, k_d, between the two R_m cases are highly distinguishable; the high R_m case has a more distinct non-Gaussian distribution. The large deviation from a Gaussian distribution at k_* and k_d scales for the high R_m case indicates that turbulence is highly intermittent at those scales. Both Figs. 5(a) and 5(b) help explain the plasmoid formation in the elongated and intense current sheets despite the statically moderate values of the alignment angle.

Conclusions.—In this Letter, we show, via direct numerical simulations, that the plasmoid instability can modify the MHD turbulent cascade for sufficiently large magnetic Reynolds numbers. For the higher magnetic Reynolds
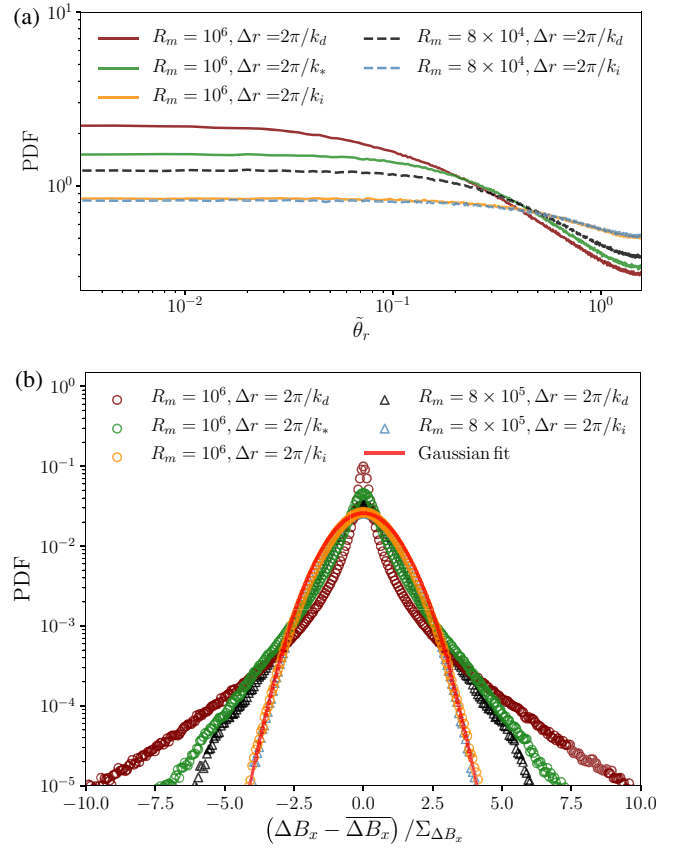

FIG. 5. PDFs of (a) the alignment angle $\tilde{\theta}_r$ and (b) $(\Delta B_x - \overline{\Delta B_x})/\Sigma_{\Delta B_x}$ ($\Sigma_{\Delta B_x}$ the standard deviation of ΔB_x) at different separations determined by k_i, k_*, and k_d as indicated in Fig. 3. (a) $\tilde{\theta}_r$ has a relatively uniform distribution at the k_i scale for both R_m cases. At the k_d scale, the high R_m case exhibits higher nonuniformity than the low R_m case. (b) At the k_i scale, both R_m cases show similar PDFs that can accurately fit the Gaussian distribution. The PDFs at k_d between low and high R_m cases are clearly distinguishable; the latter deviates more from the Gaussian distribution.

number considered ($R_m = 1 \times 10^6$), the energy spectrum steepens relative to the inertial range when the plasmoid instability becomes effective in disrupting current sheets. This occurs at relatively small scales, where the combined effects of dynamic alignment and intermittency produce current sheets more prone to the plasmoid instability. In this plasmoid-mediated regime, we found that the magnetic energy spectrum exhibits a spectral index close to -2.2. Therefore, the disruption of current sheets due to the plasmoid instability facilitates the energy cascade toward small scales.

To quantify the effect of the dynamic alignment, we measured the alignment angle θ_r, which decreases toward small scales with a slope that is approximately captured by the scaling $\theta_r \propto \Delta r^{0.25}$. This is analogous to what is found in 3D MHD turbulence, thus suggesting a possible common explanation underlying this behavior. Despite the fact that the dynamic alignment can be related to the

increase of the aspect ratio of current sheets, for the magnetic Reynolds number investigated here it is not sufficient to explain the plasmoid formation per se. However, intensified nonuniformity in θ_r and significantly non-Gaussian distribution of magnetic field increments are shown to occur at smaller scales for the case with a high R_m, which may suffice to reach the critical current sheet aspect ratio required for the formation of plasmoids within the typical eddy turnover time.

The alignment angle θ_r is not affected by the development of plasmoids in our simulations, in contrast to the theoretical predictions of Refs. [38,39]. A possible explanation is that the plasmoids start to form and evolve at moderate values of θ_r with the assistance of intermittency. The impact of the plasmoid instability in modifying the dynamic alignment could become manifest at larger R_m, where the anisotropy becomes significantly larger. Furthermore, it is shown in Ref. [39] that the plasmoid-mediated regime cannot be characterized by a true power law due to the nature of the plasmoid instability in time-evolving current sheets. This phenomenon seems to be captured by our numerical simulations based on the adopted R_m. However, significantly larger R_m values are required to see a more clear and broader trend.

Several questions remain open, e.g., the role of dimensionality (2D vs 3D) on intermittency and energy transfer between scales, the difference between decaying turbulence and forced turbulence, and how to examine different existing theories against numerical simulations.

*dcfy@princeton.edu

[1] W. H. Matthaeus, G. P. Zank, S. Oughton, D. J. Mullan, and P. Dmitruk, Astrophys. J. **523**, L93 (1999).

[2] S. R. Cranmer, A. A. van Ballegooijen, and R. J. Edgar, Astrophys. J. **171**, 520 (2007).

[3] S. A. Balbus and J. F. Hawley, Rev. Mod. Phys. **70**, 1 (1998).

[4] A. Brandenburg and K. Subramanian, Phys. Rep. **417**, 1 (2005).

[5] J. W. Armstrong, B. J. Rickett, and S. R. Spangler, Astrophys. J. **443**, 209 (1995).

[6] B. G. Elmegreen and J. Scalo, Annu. Rev. Astron. Astrophys. **42**, 211 (2004).

[7] E. G. Zweibel and C. Heiles, Nature (London) **385**, 131 (1997).

[8] F. Miniati and A. Beresnyak, Nature (London) **523**, 59 (2015).

[9] D. Biskamp and H. Welter, Phys. Fluids B **1**, 1964 (1989).

[10] H. Politano, A. Pouquet, and P. L. Sulem, Phys. Plasmas **2**, 2931 (1995).

[11] D. Biskamp, *Magnetohydrodynamic Turbulence* (Cambridge University Press, Cambridge, England, 2003), DOI: 10.1017/CBO9780511535222.

[12] D. Biskamp and E. Schwarz, Phys. Plasmas **8**, 3282 (2001).

[13] P. D. Mininni, A. G. Pouquet, and D. C. Montgomery, Phys. Rev. Lett. **97**, 244503 (2006).

[14] V. Zhdankin, D. A. Uzdensky, J. C. Perez, and S. Boldyrev, Astrophys. J. **771**, 124 (2013).

[15] M. Wan, A. F. Rappazzo, W. H. Matthaeus, S. Servidio, and S. Oughton, Astrophys. J. **797**, 63 (2014).

[16] K. D. Makwana, V. Zhdankin, H. Li, W. Daughton, and F. Cattaneo, Phys. Plasmas **22**, 042902 (2015).

[17] W. H. Matthaeus, M. Wan, S. Servidio, A. Greco, K. T. Osman, S. Oughton, and P. Dmitruk, Phil. Trans. R. Soc. A **373**, 20140154 (2015).

[18] J. Mak, S. D. Griffiths, and D. W. Hughes, Phys. Rev. Fluids **2**, 113701 (2017).

[19] Y. Yang, W. H. Matthaeus, Y. Shi, M. Wan, and S. Chen, Phys. Fluids **29**, 035105 (2017).

[20] W. H. Matthaeus and S. L. Lamkin, Phys. Fluids **29**, 2513 (1986).

[21] H. Politano, A. Pouquet, and P. L. Sulem, Phys. Fluids B **1**, 2330 (1989).

[22] M. L. Goldstein, D. A. Roberts, and W. H. Matthaeus, Annu. Rev. Astron. Astrophys. **33**, 283 (1995).

[23] S. Servidio, W. H. Matthaeus, M. A. Shay, P. A. Cassak, and P. Dmitruk, Phys. Rev. Lett. **102**, 115003 (2009).

[24] S. Servidio, P. Dmitruk, A. Greco, M. Wan, S. Donato, P. A. Cassak, M. A. Shay, V. Carbone, and W. H. Matthaeus, Nonlinear Processes Geophys. **18**, 675 (2011).

[25] M. Wan, W. H. Matthaeus, S. Servidio, and S. Oughton, Phys. Plasmas **20**, 042307 (2013).

[26] Y.-M. Huang and A. Bhattacharjee, Astrophys. J. **818**, 20 (2016).

[27] S. S. Cerri and F. Califano, New J. Phys. **19**, 025007 (2017).

[28] L. Franci, S. S. Cerri, F. Califano, S. Landi, E. Papini, A. Verdini, L. Matteini, F. Jenko, and P. Hellinger, Astrophys. J. Lett. **850**, L16 (2017).

[29] L. Franci, S. Landi, A. Verdini, L. Matteini, and P. Hellinger, Astrophys. J. **853**, 26 (2018).

[30] V. Carbone, P. Veltri, and A. Mangeney, Phys. Fluids A **2**, 1487 (1990).

[31] F. Pucci and M. Velli, Astrophys. J. Lett. **780**, L19 (2014).

[32] L. Comisso, M. Lingam, Y.-M. Huang, and A. Bhattacharjee, Phys. Plasmas **23**, 100702 (2016).

[33] A. Tenerani, M. Velli, F. Pucci, S. Landi, and A. F. Rappazzo, J. Plasma Phys. **82**, 31 (2016).

[34] Y.-M. Huang, L. Comisso, and A. Bhattacharjee, Astrophys. J. **849**, 75 (2017).

[35] L. Comisso, M. Lingam, Y.-M. Huang, and A. Bhattacharjee, Astrophys. J. **850,** 142 (2017).

[36] A. Mallet, A. A. Schekochihin, and B. D. G. Chandran, Mon. Not. R. Astron. Soc. **468,** 4862 (2017).

[37] N. F. Loureiro and S. Boldyrev, Phys. Rev. Lett. **118,** 245101 (2017).

[38] S. Boldyrev and N. F. Loureiro, Astrophys. J. **844,** 125 (2017).

[39] L. Comisso, Y.-M. Huang, M. Lingam, E. Hirvijoki, and A. Bhattacharjee, Astrophys. J. **854,** 103 (2018).

[40] G. Toth *et al.*, J. Comput. Phys. **231,** 870 (2012).

[41] See Supplemental Material at http://link.aps.org/supplemental/10.1103/PhysRevLett.121.165101 for the evolution of plasmoids in multiple intense current sheets.

[42] P. S. Iroshnikov, Astron. Zh. **40,** 742 (1963) [Sov. Astron. **7,** 566 (1964)].

[43] R. H. Kraichnan, Phys. Fluids **8,** 1385 (1965).

[44] We also examined the kinetic energy spectra, where the incompressible and compressible components exhibit similar spectral shapes (not shown here), and manifest a clear "break" in the spectral index near $k = k_*$.

[45] It is noteworthy that various theoretical predictions for accurate values of k_* were all derived for forced turbulence, whereas in our simulations we consider decaying turbulence. In addition, the existent theoretical predictions do not take intermittency into account.

[46] S. Boldyrev, Phys. Rev. Lett. **96,** 115002 (2006).

[47] J. Mason, F. Cattaneo, and S. Boldyrev, Phys. Rev. Lett. **97,** 255002 (2006).

[48] A. Greco, P. Chuychai, W. H. Matthaeus, S. Servidio, and P. Dmitruk, Geophys. Res. Lett. **35,** L19111 (2008).